ADVANCED FUNCTIONAL MATERIALS
www.afm-journal.de

Materials Views
www.MaterialsViews.com

Self Encapsulated Poly(3-hexylthiophene)-poly(fluorinated alkyl methacrylate) Rod-Coil Block Copolymers with High Field Effect Mobilities on Bare SiO_2

*Junying Liu, Dahlia Haynes, Courtney Balliet, Rui Zhang, Tomasz Kowalewski, and Richard D. McCullough**

Conjugated rod-coil block copolymers provide an interesting route towards enhancing the properties of the conjugated block due to self-assembly and the interplay of rod-rod and rod-coil interactions. Here, we demonstrate the ability of an attached semi-fluorinated block to significantly improve upon the charge carrier properties of *regioregular* poly(3-hexyl thiophene) (*rr*-P3HT) materials on bare SiO_2. The thin film hole mobilities on bare SiO_2 dielectric surfaces of poly (3-hexyl thiophene)-*block*-polyfluoromethacrylates (P3HT-*b*-PFMAs) can approach up to 0.12 $cm^2 V^{-1} s^{-1}$ with only 33 wt% of the P3HT block incorporated in the copolymer, as compared to *rr*-P3HT alone which typically has mobilities averaging 0.03 $cm^2 V^{-1} s^{-1}$. To our knowledge, this is the highest mobility reported in literature for block copolymers containing a P3HT. More importantly, these high hole mobilities are achieved without multistep OTS treatments, argon protection, or post-annealing conditions. Grazing incidence wide-angle x-ray scattering (GIWAX) data revealed that in the P3HT-*b*-PFMA copolymers, the P3HT rod block self-assembles into highly ordered lamellar structures, similar to that of the *rr*-P3HT homopolymer. Grazing incidence small-angle x-ray scattering (GISAXS) data revealed that lamellar structures are only observed in perpendicular direction with short PFMA blocks, while lamellae in both perpendicular and parallel directions are observed in polymers with longer PFMA blocks. AFM, GIWAXS, and contact angle measurements also indicate that PFMA block assembles at the polymer thin film surface and forms an encapsulation layer. The high charge carrier mobilities and the hydrophobic surface of the block copolymer films clearly demonstrates the influence of the coil block segment on device performance by balancing the crystallization and microphase separation in the bulk morphological structure.

1. Introduction

The design and development of organic and polymeric semiconductors as active components in field effect transistor (FET) devices has garnered tremendous interest as a replacement for inorganic based electronic materials in both academic and commercial arenas. The discovery of π-conjugated organic molecules and polymers has promoted a widespread interest in investigating potential optoelectronic industries as they offer unique advantages over traditional non-organic materials due to their lightweight, low cost, facile synthetic strategies, solution processability, ease of fabrication and flexible attributes.[1–3] Among the parameters necessary to achieve high performance OFETs, one of the most crucial relies on the ability to control the morphology of nanometer and micrometer sized structures, and the π conjugation and connectivity via polymer engineering and processing conditions.[4–9] This aforementioned capability to control self-assembly of nano-structured materials plays a prevalent role towards the development of highly optimal electronic devices. To this end, a large number of research groups have investigated the self-assembly of organic molecules and polymers through various synthetic methodologies and one of the most common techniques, employs the use of block copolymers that can undergo self-assembly and offer control over nanoscale morphologies.[10–15]

In particular, conjugated rod-coil block copolymers is of great appeal since it provides a simple route towards achieving a diverse array of nanostructures and thus offers control over π conjugation and connectivity via self-assembly into a number of nanoscale morphologies.[16–19] Such block copolymers combine the advantages of conducting and insulating polymers, resulting in materials with desirable functions, such as enhanced electronic and mechanical properties.[20–24] The inherent tunability of block copolymers will allow us to control device performance by structure design, allowing for the adjustment of one block in the copolymer, which can be used to balance or influence the properties of the other block dependent on the end-use application. Furthermore, rod-coil block copolymers have shown preferential ordering of one block over the other at specific interfaces during film formation.[25] This unique ability can be exploited to enhance

J. Liu, Dr. D. Haynes, C. Balliet, Dr. R. Zhang, Prof. T. Kowalewski, Prof. R. D. McCullough
Dept. of Chemistry
Carnegie Mellon University
4400 Fifth Avenue, Pittsburgh, PA 15213, USA
E-mail: rm5g@andrew.cmu.edu

DOI: 10.1002/adfm.201102431

the microphase separation and self-assembly of the organic materials that is necessary for electronic devices.

Regioregular poly(3-hexythiophene) (*rr*-P3HT) is currently the most widely used organic semiconducting polymer for OFETs due to its good solubility, chemical stability, high charge carrier mobility, and ease of syntheses.[1,2,26–32] Rod-coil block copolymers containing *rr*-P3HT as the rod with different coil segments have been widely studied and a variety of different nanoscale patterns have been achieved upon altering of the non-conjugated coil block, block length or block composition.[12,33–37] Fluorinated compounds has a number of unique properties that as incorporated into the coil segment of a block copolymer, can provide great thermal and oxidative stability, hydrophobicity, and high resistance to chemicals that may positively influence the properties of the covalently attached rod moiety.[38–42] In addition, the immiscibility with carbon–hydrogen groups and the F…H–C interactions play an important role in solid state organization.[43] For example, by incorporating semifluoroalkyl derivatives in poly(3-thiophene) side chains, the resulting polymer films were shown to assemble into highly ordered bilayer lamellar structures due to the segregation of the hydrocarbon and fluorocarbon chains. The resultant polymers also showed good charge carrier mobilities (μ ~ 0.0145 cm^2 V^{-1} s^{-1}).[44] In another example, the electrochemical polymerization of perfluoroalkyl substituted thiophene resulted in super water- and oil-repellent polythiophene films due to migration of the fluorinated segment to the surface of the thin films.[45]

Accordingly, incorporating fluorinated moieties as the coil segment of rod-coil block copolymers are expected to provide interesting properties and advantageous morphologies for optoelectronic devices. Due to the low surface energy of fluorinated compounds, it is possible that the fluorinated segments in a conducting block copolymer would preferentially align at the air surface of the polymer thin film, thus acting as an encapsulating layer thereby providing polymers with increased resistance to oxygen, moisture, heat and chemicals. In addition, the strong incompatibility of fluorine groups with conventional hydrocarbon-based derivatives may cause fluorine segments to self-aggregate, resulting in polymers with interesting morphology and enhanced electronic properties.

In this paper, fluorinated alkyl methacrylates are covalently attached to *rr*-P3HT forming rod-coil block copolymers (P3HT-*b*-PFMAs) by the combination of GRIM polymerization methods and controlled radical polymerizations. We demonstrate the effect of the fluoromethacrylate on rr-P3HT as P3HT-*b*-PFMA thin films exhibit surprisingly high charge carrier mobilities. The hole mobilities can approach 0.12 cm^2 V^{-1} s^{-1} on a bare SiO_2 dielectric surfaces with only 33wt% of P3HT incorporated in the copolymers, which is much higher than *rr*-P3HT (0.03 cm^2 V^{-1} s^{-1}) measured under the same conditions. More importantly, the mobilities of P3HT-*b*-PFMA block copolymers increased as the weight composition of the insulating PFMA blocks increased. The thin film bulk microstructure of the P3HT-*b*-PFMA copolymers was investigated using GIXs spectroscopy. P3HT rod blocks self-assemble into highly ordered lamellar configurations, typical of what occurs for *rr*-P3HT homopolymers. Dependent upon the length of the PFMA chain, GISAXS revealed that lamellae morphology is enhanced in both the parallel and perpendicular directions with an increase in fluorine composition. The high hole mobilities and the hydrophobic surface of the block copolymers clearly demonstrate the tunability of the device performance by introducing a fluorinated matrix.

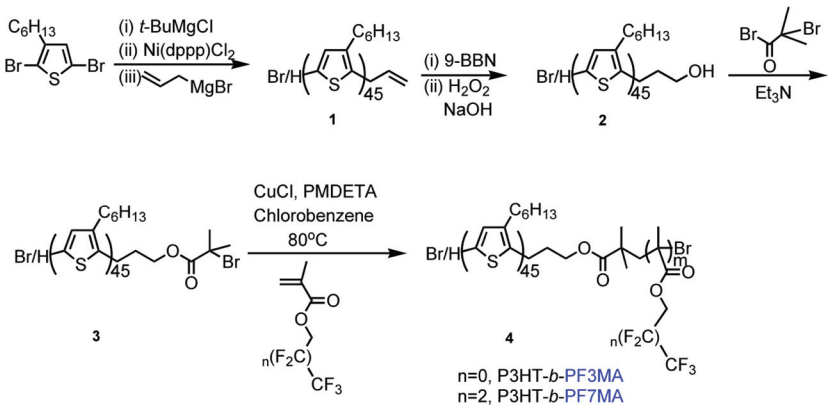

Scheme 1. Synthetic route for P3HT-*b*-PFMAs.

2. Results and Discussion

P3HT-*b*-PFMAs rod-coil block copolymers were synthesized via the "grafting-from" method using a P3HT macroinitiator. The P3HT blocks were synthesized by controlled Grignard Metathesis (GRIM) polymerizations and subsequently end capped with an allyl group.[21a,46] The allyl end group was then converted into the corresponding bromoester initiator according to previously reported procedures,[12,34] followed by controlled atom transfer radical polymerizations (ATRP) of fluorinated methacrylates to generate a series of P3HT-*b*-PFMAs (**Scheme 1**). By using ATRP,[47] the molecular weight of the fluorinated methacrylate segment was controlled by the molar ratio of monomer polymerized relative to the polythiophene macroinitiator. Thus, by collecting samples at different reaction times during ATRP, a series of P3HT-*b*-PFMA block polymers with the same P3HT block and different PFMA fractions were obtained (**Table 1**).

Table 1. Properties of P3HT-b-PFMAs.

Polymer	Wt% of P3HT[a)]	Mn [g.mol^{-1}][b)]	PDI[b)]
P3HT-b-PF3MA	100	11000	1.1
	64	16800	1.3
	41	20130	1.4
	26	22200	1.6
P3HT-b-PF7MA	100	11000	1.1
	54	16680	1.2
	45	17100	1.3
	33	17250	1.4

[a)]Determined by ^{1}H NMR; [b)]Determined by GPC relative to polystyrene standards

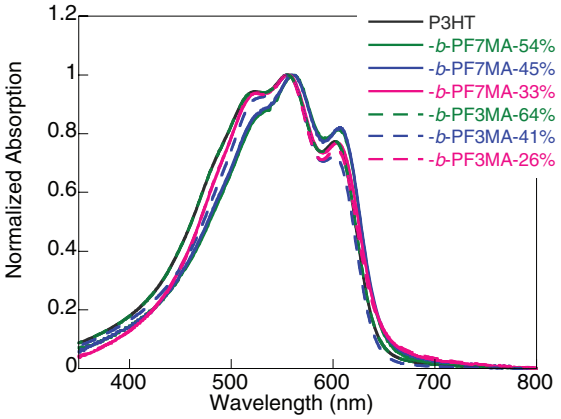

Figure 1. UV–vis absorption of P3HT-b-PFMA block copolymers in films

To determine how the fluorine content in the coil block affects polymer properties, two different fluoromethacrylate compositions (P3HT-*b*-PF3MAs and P3HT-b-PF7MAs) were synthesized (Scheme 1).

The chemical structure and the molar ratio of the different P3HT-*b*-PFMAs block copolymers were confirmed by ^{1}H and ^{19}F NMR spectroscopy (Supporting Information (SI) Figure SI1 and SI2). A DPn of 45 (Mn ~ 7.4 kg/mol) for the P3HT macroinitiators was determined by ^{1}H NMR (Figure SI3), and the integration of the PFMA resonances in respect to the P3HT resonances allowed for quantitative determination of the PFMA block length. Based on these NMR calculations, the weight percentage of the P3HT and PFMA block can be calculated. In addition, the molecular weight of the corresponding polymers was also tested using GPC (polystyrene as standard) and the results are listed in Table 1. All P3HT-*b*-PFMAs are readily soluble in chloroform at room temperature and forms very uniform films through drop casting and spin coating.

Spectroscopic characterization, in particular UV–vis of conjugated polymers can provide unique information about structural order and intermolecular (π–π) interactions in solid-state.[48–51] The UV–vis absorption measurements of the block polymers can reveal the influence of the coil segment on the optoelectronic properties of the conjugated moiety, and in addition, can reveal the structural order of the block copolymers. Since the PFMA segments do not absorb in the visible region; the features of the spectra are attributed to polythiophene block. In chloroform solutions, the block copolymers exhibit the same absorption spectra as that of *rr*-P3HT with λ_{max} at 455nm. The absorption of P3HT-*b*-PFMAs thin films drop casted from chloroform solutions exhibited λ_{max} at 575nm with strong vibrational peaks at 615 nm (**Figure 1**). These features are similar to those observed in *rr*-P3HT, which strongly suggest that in the solid state, the coil like nature of the PFMA segment does not interrupt the strong π–π stacking interactions of the P3HT moiety, thus maintaining the highly ordered structures.[52–54] The bathochromic shift found between the solutions and solid-state spectra is due to enhanced interchain association in the solid state.[5]

The fluorinated coil block (PFMA) effects on the polymer surface properties were studied by water contact angle measurements and AFM. The thin films were prepared by drop casting 1mg/mL polymer $CHCl_3$ solutions on bare SiO_2 wafers, and measurements were made at different sites across the film surface in order to assess its homogeneity. The water contact angle of P3HT-*b*-PF3MA showed values in the range of 100–103°, slightly higher than the water contact angle of *rr*-P3HT homopolymer (95–98°), while the increased fluorine content of the P3HT-b-PF7MA block copolymer exhibited a higher level of hydrophobicity (113–115°) (vida infra **Figure 2**). For P3HT-*b*-PF3MA, the lower fluorine content does not significantly effect the nanofibrillar formation of the *rr*-P3HT block as the TMAFM revealed smaller but similar fibril-like microstructures. The morphological and contact angle studies indicate that some of the fluorinated segments orient to the film and air interface, thus decreasing surface tension. Increase of the fluorine content (P3HT-*b*-PF7MA) in the coil block dramatically alters the thin film morphology giving a cauliflower-like microstructure, completely suppressing nanofibrillar formation on the surface. In comparison with the P3HT-*b*-PF3MA, the rougher surface can be attributed to increased hydrophobicity, with water contact angles of 113–115°. This observation clearly indicates that the fluorinated coil segment in the P3HT-*b*-PF7MA preferentially segregates at the thin film surface, resulting in a directed self-encapsulation layer of the rod-coil block copolymer and as such can provide opportunities for applications that require moisture repellent properties.

The nano- and microstructure of self-assembled block copolymers plays a crucial role in controlling FET device performances. The strong lamellar and pi-stacking of *rr*-P3HT allows for detailed analysis of the microstructures using grazing incidence wide-angle x-ray scattering (GIWAXS) and grazing

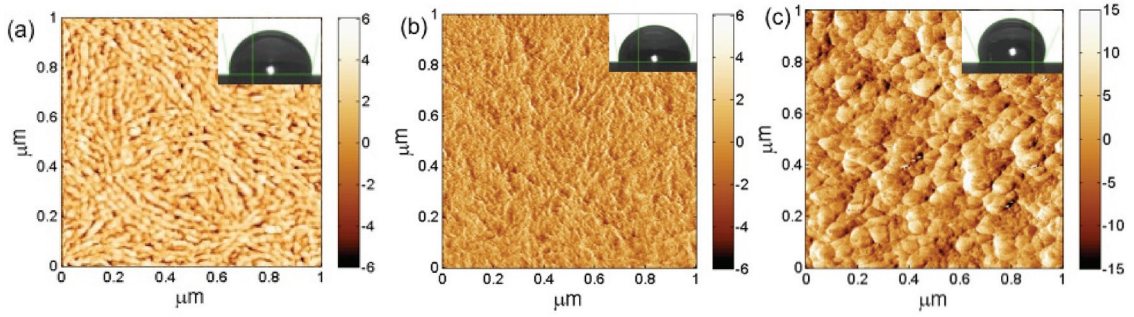

Figure 2. AFM images of a) rr-P3HT, b) P3HT-*b*-PF3MA containing 26wt% P3HT, c) P3HT- *b* -PF7MA containing 33wt% P3HT. Insets: camera images of a water droplet on the film.

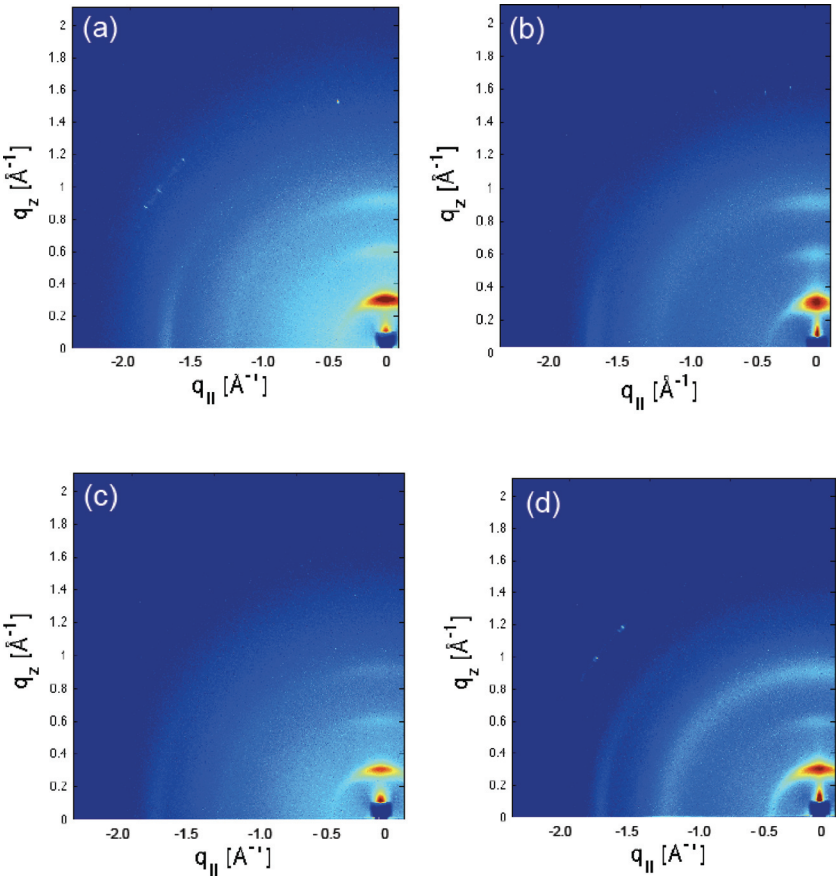

Figure 3. Two-dimensional GIWAXS images of P3HT-*b*-PF3MA copolymers on bare SiO_2/Si substrate; a) with 64wt% P3HT, b) with 26wt% P3HT; images of P3HT- *b* -PF7MA copolymers c) with 54wt% P3HT, d) with 33 wt% P3HT.

incidence small-angle x-ray scattering (GISAXS), therefore the influence of the PFMA segment on the P3HT domains should be readily observed.

GIWAXS patterns of as cast P3HT-*b*-PFMA thin films are shown in **Figure 3**. The films showed pronounced molecular layering (*100, 200, 300*) along the q_z direction, analogous to that of *rr*-P3HT with inter-sheet spacing of ~16.1 Å for P3HT-*b*-PF3MA and 16.3 Å for P3HT-*b*-PF7MA, respectively. The weak arc along the q_{xy} direction in the GIWAXS spectrum can be assigned to the π–π stacking of the P3HT block edge-on with the substrate having a *d* spacing of 3.9 Å for both P3HT-*b*-PF3MAs and P3HT-*b*-PF7MAs. The weak, broad peak at q = 1.2 Å^{-1} corresponds to the scattering from PFMA segments, which get stronger with longer PFMA segments. The GIWAXS patterns of P3HT-*b*-PFMAs are similar to those of *rr*-P3HT homopolymers, indicating that the fluoromethacrylates did not significantly influence the microstructure organization of the rod P3HT block and it self-assembles into highly ordered lamellar structures. Thus, the highly ordered P3HT block will still facilitate charge carrier transport in the block copolymers.

Close examination of GIWAXS revealed the improvement of polymer microstructures with increasing fractions of the insulating PFMA segments. For P3HT-*b*-PF3MA polymers, the normalized angular intensity profiles of the (*100*) peak for polymer with 26wt% P3HT block exhibited much narrower azimuthal angle range than polymer with 64wt% P3HT block (Figure SI4), which revealed its better oriented lamellar structure with increase PF3MA block in the polymer. This improvement in turn facilitats the in-plane charge transport. In the case of P3HT-*b*-PF7MA, the more intense *(200), (300),* and the π–π stacking peaks for the polymer with higher PF7MA fractions clearly indicates a stronger ordering in the microstructure (Figure SI5). This structure improvement with longer PFMA segments may be related to the strong incompatibility of fluorine groups with hydrocarbon-based polymers, which causes the fluorine segment to self-aggregate and forces the P3HT into a more crystallizable and ordered position. This incompatibility promotes the assembly of the conducting block and offers insight into the improved charge carrier mobility.

While GIWAXS is used to investigate the thin film microstructures with periodicities ranging from 1 to 100 Å; GISAXS is mainly used to examine nanoscale structure correlations.[55] Interestingly, GISAXS analysis revealed that the morphology of P3HT-*b*-PFMAs changes as a function of PFMA block length. For P3HT-*b*-PFMA with shorter PFMA segments, only in-plane scattering peaks (q_{xy}) are observed, characteristic of lamellar perpendicular to the substrate. Remarkably, increasing the weight ratio of PFMA segments results in the appearance of both in plane (q_{xy}) and out of plane (q_z) scattering peaks in GISAXS. These features indicate the appearance of lamellae on both perpendicular and parallel to the substrate. The morphological changes for P3HT-*b*-PFMAs as a function of the PFMA block is demonstrated in the proposed model (**Figure 4**e). For P3HT-*b*-PF7MA, the appearance of the vertical phase separation together with the AFM image from Figure 2c, clearly indicate the capability of P3HT-*b*-PF7MA copolymers forming a "self-encapsulation" layer.

The effect of the insulating PFMA coil block on the electrical properties of the block copolymers were investigated and provided interesting results on the preservation of continuous charge transport despite the varied microstructure changes of P3HT seen in GIWAXs and GISAXs analyses. Both the bulk electrical conductivity and charge carrier mobilities at the device interface of the copolymers were evaluated. The electrical conductivities were measured using the four-point probe technique and film thickness was measured by profilometry. As shown in **Figure 5**, P3HT-*b*-PFMAs exhibited high conductivity even with a low fraction of P3HT (26 wt%) incorporated into the polymer. This high conductivity may be attributed to the P3HT block self-assembling into conducting nanofibrils that provide pathways for charge carriers that is consistent in

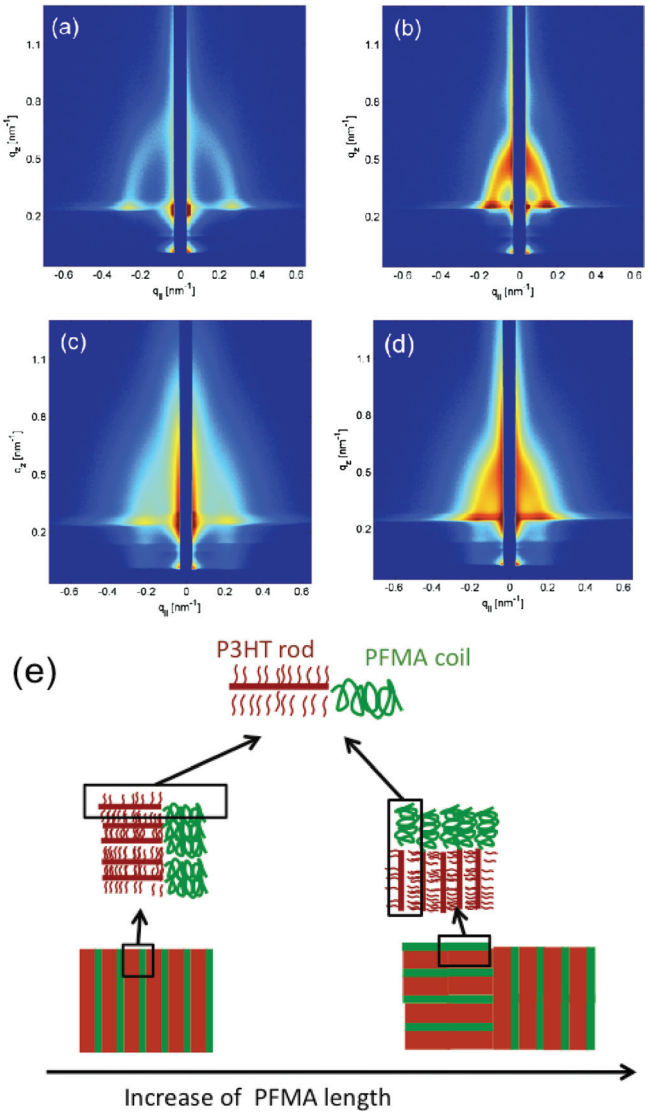

Figure 4. GISAXS patterns of P3HT-*b*-PFMA. a) P3HT-*b*-PF3MA containing 64wt%P3HT; b) P3HT-*b*-PF3MA containing 26wt% P3HT; c) P3HT-*b*-PF7MA containing 54wt%P3HT; d) P3HT-*b*-PF7MA containing 33wt%P3HT; e) Proposed model for the structure changes.

previous results, both in P3HT homo- and co-polymer thin films.[33] As expected, polymer conductivity decreased as the insulating PFMA segment of the copolymer increased. This is attributed to the increase of the insulating segment in the block copolymer "diluting" the current density of the film, thus decreasing its bulk conductivity.

Bottom-gate and bottom-contact field-effect transistor devices were used to evaluate field-effect transistor performances. Polymer thin films were deposited by drop casting from chloroform solutions under ambient conditions on SiO_2 dielectric surfaces without the multistep OTS treatment, followed by vacuum drying overnight. The field effect mobilities were measured in air and calculated from transfer curves taken in the saturation regime. In the saturated region, mobility is calculated based on the following equation. Here, V_T is the threshold

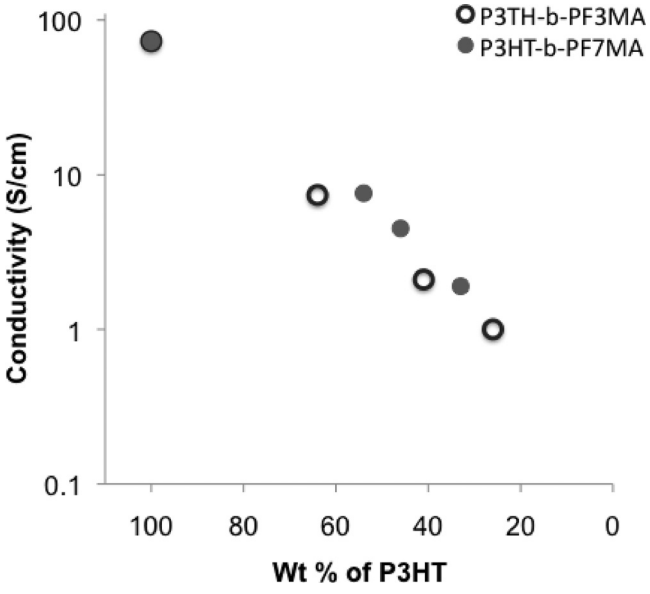

Figure 5. Conductivities of P3HT-*b*-PFMA as a function of weight content of P3HT block

voltage at which the current starts to rise. C is the capacitance of the gate dielectric, and W and L are the width and length of the conducting channel.

$$I_D = \frac{W}{2L}\mu C(V_G - V_T)^2$$

In all cases, mobility data were obtained from at least eight different films using transistors with channel lengths from 15 μm to 40 μm to avoid short channel effects and negate the effects of thin film samples variations. **Figure 6** shows a representative current-voltage transfer curve at drain-source voltage (V_{DS}) –80 V and an output curve of FETs fabricated with P3HT-*b*-PFMA copolymer solutions. The mobility of the block copolymers as a function of weight content of P3HT is shown in **Figure 7**.

Interestingly, P3HT-*b*-PFMA thin films exhibited high charge carrier mobilities, with average mobilities above 0.09 $cm^2\ s^{-1}\ V^{-1}$ and $I_{on/off}$ of 10^2. In addition, as clearly seen from Figure 5, the mobilities of P3HT-*b*-PFMA increased for longer PFMA insulating segments. This increase in field effect mobilities may be understood by observing the morphological changes as a function of increased fractions of PFMA as shown in GISAXS (Figure 4). While, only nanofibrillar structures were observed in polymers with shorter PFMA segments, both nanofibrillar structures and parallel layer microstructures were generated with the longer PFMA segments. This parallel layer structure may, in fact decrease the insulating PFMA segment density at the polymer/dielectric interface. Since charge carriers traveling through the conductive channel had to move from one crystallite to another through intervening layers of insulating PFMA segments, decreasing the density of the insulating PFMA segment at the polymer/ dielectric interface will result in increased mobility.[56,57] In addition, the improved charge carrier mobility may also be associated with improved molecular ordering of the P3HT segment as the molar composition of the insulating block increased as revealed by GIWAXS.

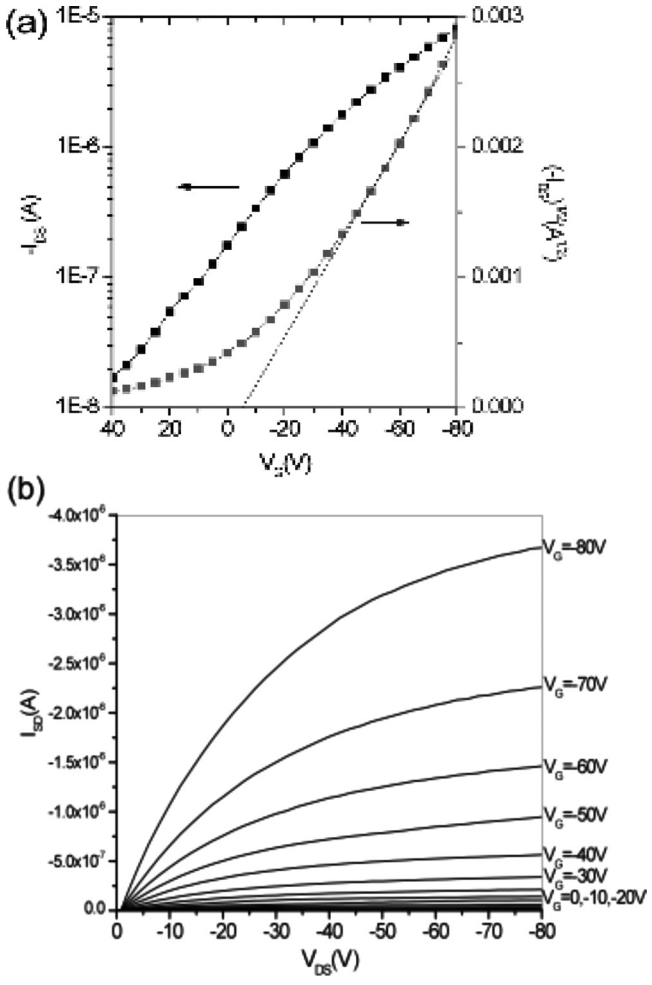

Figure 6. Current–voltage characteristics of P3HT-*b*-PF3MA containing 41 wt% P3HT on bare SiO_2 dielectric surface. a) Transfer curve at V_{DS} = –80 V, b) output curves at different gate voltage. (The extracted mobility was 0.036 cm^2 V^{-1} S^{-1}. The channel length was 40 μm and the channel width was 250 μm)

Remarkably, the mobility of P3HT-*b*-PF7MA approaches up to 0.12 cm^2 s^{-1} V^{-1} on a bare SiO_2 dielectric surface for P3HT-*b*-PF7MA with 33wt% P3HT in the block, which is much higher than field-effect mobilities of *rr*-P3HT 0.03 cm^2 s^{-1} V^{-1} measured under the same conditions (Figure SI6). Combining the AFM, GIWAXS, and GISAXS study, we demonstrate that the high charge carrier mobility is significantly influenced by the PF7MA block to aggregate at the thin film air/surface interface resulting in hydrophobic surfaces and consequently pushes the P3HT block towards the dielectric interface. In addition, the incompatibility of fluorinated coil block with the hydrocarbon-based P3HT block promotes the self-assembly of the P3HT block, and thus results in even higher mobility than *rr*-P3HT.

3. Conclusions

In summary, we have successfully synthesized P3HT-*b*-PFMAs rod-coil diblock copolymers with excellent field effect transistor

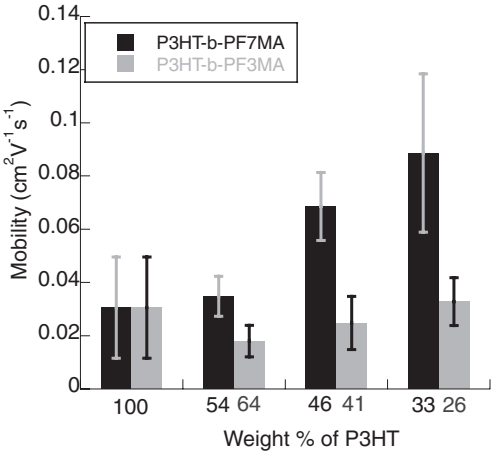

Figure 7. Charge carrier mobility of P3HT-*b*-PFMA as a function of the weight content of P3HT block

performances and increased water repellent properties, compared to that of *rr*-P3HT. The fluorinated methacrylate coil block increased the polymer thin film hydrophobicity and acted as a self-encapsulation layer. More importantly, P3HT-*b*-PFMA thin films exhibited very high charge carrier mobilities, despite the low molecular weight of the conduction block. Charge carrier mobilities can reach 0.12 cm^2 V^{-1} s^{-1}, with an average of 0.09 cm^2 V^{-1} s^{-1} on bare SiO_2 dielectric surfaces without thermally annealing or post treatment conditions, much higher than that of *rr*-P3HT with similar molecular weight. The influence of fluorine content on charge carrier mobilities and the hydrophobicity of thin film surfaces of the block copolymers clearly demonstrate the tunability of the device performance by the block copolymer structure.

4. Experimental Section

Materials. 2,5-dibromo-3-hexylthiophene was prepared according to literature.[27] *t*-butyl magnesium chloride, allyl magnesium chloride, 2,2,3,3,4,4,4-heptafluorobutyl methacrylate, 2,2,2-Trifluoroethyl methacrylate, *N*,*N*,*N*′,*N*″,*N*″-pentamethyldiethylenetriamine, and triethylamine are purchased from sigma-aldrich and used without further purification.

4.1. Polymer Synthesis

Allyl-Terminated Poly(3-hexylthiophene) (1): A dry 250 mL three-neck flask was flushed with nitrogen and was charged with 2,5-dibromo-3-hexylthiophene (5.318 g, 16.31 mmol) and anhydrous THF (8 mL). A 2 M *t*-butyl magnesium chloride (8.16 mL, 16.31 mmol) in diethyl ether (Et_2O) was added via a syringe, and the reaction stirred at room temperature for 90 min. Then anhydrous THF (160 mL) was added to dilute the solution, followed by the addition of Ni(dppp)Cl_2 (0.123 g, 0.227 mmol). The polymerization was allowed to proceed for 10 min at room temperature followed by the addition of a 1 M solution of allyl magnesium bromide (3.26 mL, 3.26 mmol). The reaction mixture was stirred for 5 min and then quenched with methanol. The precipitate was filtered and extracted with methanol, hexanes, and chloroform. Polymer was characterized by ^1H NMR.

Hydroxypropyl-Terminated Poly (3-Hexylthiophene) (2): A dry 500 mL three-neck flask was flushed with nitrogen and was charged with allyl-terminated poly(3-hexylthiophene) (1 g, 0.13 mmol), and then anhydrous THF (130 mL) was added. The reaction was stirred at 60–64° to dissolve the polymer. To this reaction mixture, a 0.5 M solution of 9-BBN (13 mL, 6.5 mmol) in anhydrous THF was added via a syringe. The reaction mixture was stirred for 24 h at 60 °C, at which point a 6 M solution of NaOH (13 mL) was added to the reaction flask. The reaction mixture was stirred for another 15 min (at which point the oil bath was removed). The reaction mixture was allowed to cool down to room temperature followed by addition of a 33% aqueous solution of hydrogen peroxide (13 mL), and the reaction was allowed to proceed for additional 12 h at 40 °C. The hydroxy-terminated polymer was isolated by precipitation in a methanol–water mixture. The polymer was filtered and purified by a Soxhlet extraction with methanol. Polymer was characterized by ^{1}H NMR.

Bromoester-Terminated Poly(3-Hexylthiophene) (3): A dry 250 mL three-neck flask was flushed with nitrogen and was charged with hydroxypropyl-terminated poly(3-hexylthiophene) (0.83 g, 0.094 mmol), and then anhydrous THF (100 mL) was added. The reaction was stirred at 60–64 °C to dissolve the polymer. Then the reaction was cooled to 40 °C. At this point, triethylamine (0.789 mL, 5.66 mmol) and a dropwise addition of 2-bromoisobutyryl bromide (0.583 mL, 4.72 mmol) were added via a syringe. The resulting poly(3-hexylthiophene) macroinitiator was precipitated in methanol and washed with cold methanol (250 mL), followed by drying under vacuum for 24 h. Polymer was characterized by ^{1}H NMR.

ATRP of Methacrylates Using Poly(3-Hexylthiophene) Macroinitiator: A dry 25mL Schlenk flask was charged with P3HT macroinitiator (0.601 g, 0.0706 mmol) and chlorobenzene (5.00 mL). The reaction was stirred at 50 °C to dissolve the macroinitiator. Then DMF (0.15 mL), 2,2,2-trifluoroethyl methacrylate (2.5 mL, 17.56 mmol), and CuCl (6.99 mg, 0.0706 mmol) were added to the reaction. After three freeze-pump-thaw cycles, the reaction mixture was immersed in a oil bath equipped with a thermostat at 80 °C. At this point, PMDETA (13.75 µL, 0.065 mmol) was added to the reaction mixture via a deoxygenated syringe and an initial sample was removed. Samples were periodically withdrawn from the reaction mixture to follow conversion and the molecular weight.

A dry 25mL Schlenk flask was charged with P3HT macroinitiator (0.601 g, 0.0706 mmol) and chlorobenzene (7.06 mL). The reaction was stirred at 50 °C to dissolve the macroinitiator. Then DMF (0.15mL), 2,2,3,3,4,4,4-heptafluorobutyl methacrylate (3.5mL, 17.56 mmol), and CuCl (6.99 mg, 0.0706 mmol) were added to the reaction. After three freeze-pump-thaw cycles, the reaction mixture was immersed in a oil bath equipped with a thermostat at 80 °C. At this point, PMDETA (13.75 µL, 0.065 mmol) was added to the reaction mixture via a deoxygenated syringe and an initial sample was removed. Samples were periodically withdrawn from the reaction mixture to follow conversion and the molecular weight.

4.2. Film Deposition

Thin films of P3HT-*b*-PFMAs were prepared by drop-casting from solvent (chloroform) onto silicon substrates. Prior to thin film deposition, the solutions were filtered through a 0.2 µm-pore-sized poly (tetrafluoroethylene) (PTFE) syringe filter. In order to facilitate equilibration of nanostructures, deposition was carried out under saturated solvent vapor by placing the substrate in a covered Petri dish partially filled with the solvent.

4.3. Polymer Characterizations

Gel permeation chromatography (GPC) was performed on a Waters 2690 separations module apparatus and a Waters 2487 dual λ absorbance detector with chloroform as the eluent (flow rate 1 mL/min, 35 °C, λ = 254 nm) and a series of three Styragel columns (10^4, 500, 100 Å; Polymer Standard Services). Toluene was the internal standard, and calibration based on polystyrene standards was applied to determine molecular weights. ^{1}H NMR spectra of the polymer solutions in $CDCl_3$ were recorded on a Bruker Avance 500 MHz spectrometer.

UV–vis: UV–vis-NIR spectra were measured on polymer solutions in anhydrous chloroform and polymer thin films cast onto 22 mm square cover glass using a UV–vis-NIR spectrophotometer (Varian Cary 5000). Electrical conductivity measurements were performed by a standard spring-loaded pressure contact Signatone S-301-4 four-point probe, which was connected to a Hewlett-Packard 6632A system dc power supply, a Hewlett-Packard 3457 A multimeter (for voltage measurements), and a Keithley model 196 system DMM (for current measurements).

Grazing Incidence Wide Angle X-ray Scattering (GIWAXS): GIWAXS images were taken at the Cornell High Energy Synchrotron Source (CHESS) D1 station. A wide bandpass (1.47%) double-bounce multilayer monochromator supplied an intense beam of 10.006 keV (l = 1.229 angstrom) photons. The beam impinged onto the sample surface at various incident angles ranging from below the critical angle of the film to above the critical angle of the substrate. The sample was mounted on a sample goniometer, in order to control the incident angle and the sample azimuth. An accurate calibration of the incident angle was performed in-situ by measuring the x-ray reflectivity from the sample using an ion chamber. GIWAXS scattering intensities were recorded with an area detector (MedOptics) with a resolution of 46.9 µm per pixel and a total area of about 50 mm by 50 mm at a distance of 98.7 mm from the sample. The intense scattering close to the direct beam was blocked with a 1.5 mm wide tantalum rod of 3 mm height. Exposures times under these conditions ranged from 1 sec to 30 sec depending on contrast and sample quality.

Grazing Incidence Small Angle X-ray Scattering (GIWAXS): The grazing incidence x-ray scattering (GIXS) images were taken at the Cornell High Energy Synchrotron Source (CHESS) D1 station. A wide bandpass (1.47%) double-bounce multilayer monochromator supplied an intense beam of 10.1 keV photons. These were impinged onto the sample surface at various incident angles ranging from below the critical angle of the film and above the critical angle of the substrate. The sample (7 mm by 7 mm) was mounted on a sample goniometer, in order to control the incident angle and the sample azimuth. An accurate calibration of the incident angle was performed in-situ by measuring the x-ray reflectivity from the sample using an ion chamber. Scattering intensities were recorded with an area detector (Medoptics) with a resolution of 47.19 µm per pixel and a total area of about 50 mm by 50 mm at distance of 1180 mm from the sample for grazing incident small angle x-ray scattering (GISAXS) analysis. The intense scattering in the incident plane was blocked with a 1.5 mm wide tantalum rod. Exposure times under these conditions ranged from 1 sec to 30 sec depending on scattering intensity of sample thin films.

Tapping Mode Atomic Force Microscopy (TMAFM): TMAFM studies were carried out with the aid of a Nanoscope III-M system (Digital Instruments, Santa Barbara, CA), equipped with a J-type vertical engage scanner. The AFM observations were performed at room temperature in air using silicon cantilevers with nominal spring constant of 50 – 80 N/m and nominal resonance frequency of ~300 kHz (standard silicon TESP probes). Typical value AFM detector signal corresponding to r.m.s. cantilever oscillation amplitude was equal to ~1000 mV and the images were acquired at 1.5 Hz scan frequency in 2 µm × 2 µm scan areas.

Electrical Conductivity Measurements: Electrical conductivity measurements were conducted on polymer thin film using four-point probe at ambient conditions. Conductivity was measured using a Signatorne Four Point Probe station and an SP4-400450RS probe, a Hewlett-Packard 6632A system DC Power Supply, and a Keithley 196 Digital Multimeter. Film thickness was measured by profilometry using an Ambios XP-2 instrument. The polymer thin films were prepared by drop casting 5g/L chloroform solution onto 22 by 22 mm glass chips, and then dried in air. The films were then doped by exposure to iodine vapors for 2 h.

4.4. Fabrication and Characterization of FET Devices

Organic field-effect transistors were fabricated in the bottom gate, bottom contact configuration on heavily-doped n-type Si substrates as the gate and a thermally grown 250 nm silicon dioxide as the dielectric layer (Silicon Quest, dry oxide). The source and drain electrodes were patterned using standard photolithography and were deposited on SiO_2 by sputter deposition of ~5 nm of titanium and 50 nm of gold. Prior to use, the devices were cleaned for 20 minutes by exposure to UV light in air (Novascan PSD-UVT) and heat (hot plate, 60 to 120 °C). Polymer films were deposited in air by drop casting 5 mL of a 1mg/mL solution in dry chloroform, and allowed to dry in a glass Petri dish saturated with chloroform. After film formation, the devices were further dried overnight in a desiccator under vacuum. Electrical measurements of the FETs were made using an Agilent 4155C Semiconductor parameter analyzer and a Micromanipulator S6 probe station. When measuring current–voltage curves and transfer curves, V_G was scanned from –80V to +40V. The field-effect mobilities were obtained from the transfer curves in the saturation regime at $V_{DS} = -80$V. A line drawn through the linear part of an $I_{DS}^{1/2}$ vs V_G plot allowed extraction of threshold voltage and field-effect mobilities using the square-law equation for the saturation regime. The average mobility was obtained from two or three transistors with channel length (L) > = 15 µm per polymer film, and for at least eight different polymer films usually cast on different days.

Supporting Information

Supporting Information is available from the Wiley Online Library or from the author.

Acknowledgements

We gratefully acknowledge National Science Foundation (CHE0415369) and Air Force Office of Scientific Research (FA9550-07-1-0245) for financial support.

Received: September 10, 2011
Revised: November 21, 2011
Published online: January 16, 2012

[1] H. Sirringhaus, N. Tessler, R. Friend, *Science* **1998**, *280*, 1741–1744.
[2] H. Sirringhaus, P. Brown, R. Friend, M. Nielsen, K. Bechgaard, B. Langeveld-Voss, A. Spiering, R. Janssen, E. Meijer, P. Herwig, D. de Leeuw, *Nature* **1999**, *401*, 685–688.
[3] B. Crone, A. Dodabalapur, Y. Lin, R. Filas, Z. Bao, A. LaDuca, R. Sarpeshkar, H. Katz, W. Li, *Nature* **2000**, *403*, 521–523.
[4] R. McCullough, *Adv. Mater.* **1998**, *10*, 93–116.
[5] J. Y. Liu, R. Zhang, G. Sauve, T. Kowalewski, R. D. McCullough, *J. Am.Chem. Soc.* **2008**, *130*, 13167–13176.
[6] I. Mcculloch, M. Heeney, C. Bailey, K. Genevicius, I. Macdonald, M. Shkunov, D. Sparrowe, S. Tierney, R. Wagner, W. Zhang, M. Chabinyc, R. Kline, M. Mcgehee, M. Toney, *Nat. Mater.* **2006**, *5*, 328–333.
[7] R. A. Segalamn, B. McCulloch, S. Kirmayer, J. J. Urban, *Macromolecules* **2009**, *42*, 9205.
[8] A. A. Virkar, S. Mannsfeld, Z. Bao, N. Stingelin, *Adv. Mater.* **2010**, *22*, 3857–3875.
[9] M. A. Baklar, F. Koch, A. Kumar, E. B. Domingo, M. Campoy-Quiles, K. Feldman, L. Yu, P. Wobkenberg, J. Ball, R. M. Wilson, I. McCulloch, T. Kreouzis, M. Heeney, T. Anthopoulos, P. Smith, N. Stingelin, *Adv. Mater.* **2010**, *22*, 3942–3947.
[10] M. Lee, B. K. Cho, W. C. Zin, *Chem. Rev.* **2001**, *101*, 3869–3892.
[11] R. A. Segalman, B. McCulloch, S. Kirmayer, J. J. Urban, *Macromolecules* **2009**, *42*, 9205–9216.
[12] C. P. Radano, O. A. Scherman, N. Stingelin-Stutzmann, C. Müller, D. W. Breiby, P. Smith, R. A. J. Janssen, E. W. Meijer, *J. Am. Chem. Soc.* **2005**, *127*, 12502–12503.
[13] C. Müller, S. Goffri, D. W. Breiby, J. W. Andreasen, H. D. Chanzy, R. A. J. Janssen, M. M. Nielsen, Radano, H. SIrringhaus, P. Smith, N. Stingelin-Stutzmann, *Adv. Func. Mater.* **2007**, *17*, 2674–2679.
[14] J. M. Hancock, A. P. Gifford, R. D. Champion, S. A. Jenekhe, *Macromolecules* **2008**, *41*, 3588–3597.
[15] P.-T. Wu, G. Ren, C. Li, R. Mezzenga, S. A. Jenekhe, *Macromolecules* **2009**, 2317–2320.
[16] F. S. Bates, *Science* **1991**, *251*, 898–905.
[17] R. A. Segalman, B. D. Olsen, *Materials Science & Engineering R-Reports* **2008**, *62*, 37–66.
[18] A. de Cuendias, R. C. Hiorns, E. Cloutet, L. Vignau, H. Cramail, *Polym. Int.* **2010**, *59*, 1452–1476.
[19] C.-L. Liu, C.-H. Lin, C.-C. Kuo, S.-T. Lin, W.-C. Chen, *Prog. Polym. Sci.* **2011**, *36*, 603–637.
[20] L. Rubatat, X. Kong, S. A. Jenekhe, J. Roukolainen, M. Hojeij, R. Mezzenga, *Macromolecules* **2008**, *41*, 1846–1852.
[21] a) R. D. McCullough, M. C. Iovu, M. Jeffries-El, E. E. Sheina, J. R. Cooper, *Polymer* **2005**, *46*, 8582–8586; b) J. S. Liu, E. Sheina, R. D. McCullough, T. Kowalewski, *Angew. Chem. Int. Ed.* **2002**, *41*, 329–332
[22] G. Ren, P. T. Wu, S. A. Jenekhe, *Chem. Mater.* **2010**, *22*, 2020–2026.
[23] X. L. Chen, S. A. Jenekhe, *Macromolecules* **2000**, *33*, 4610–4612.
[24] N. Stingelin-Stutzmann, C. Muller, S. Goffri, D. W. Breiby, J. W. Andreasen, H. D. Chanzy, R. A. J. Janssen, M. M. Nielsen, C. P. Radano, H. Sirringhaus, P. Smith, *Adv. Funct. Mater.* **2007**, *17*, 2674–2679.
[25] N. Sary, F. Richard, C. Brochon, N. Leclerc, P. Lévêque, J.-N. Audinot, S. Berson, T. Heiser, G. Hadziioannou, R. Mezzenga, *Adv. Mater.* **2010**, *22*, 763–768.
[26] C. Müller, N. D. Zhigadlo, A. Kumar, M. A. Baklar, J. Karpinski, P. Smith, T. Kreouzis, N. Stingelin, *Macromolecules* **2011**, *44*, 1221–1225.
[27] R. D. McCullough, R. S. Loewe, S. M. Khersonsky, *Adv. Mater.* **1999**, *11*, 250–253.
[28] S. Goffri, C. Müller, N. Stingelin-Stutzmann, D. W. Breiby, C. P. Radano, J. W. Andreasen, R. Thompson, R. A. J. Janssen, M. M. Nielsen, H. Sirringhaus, *Nat. Mater.* **2006**, *5*, 950–956.
[29] R. D. McCullough, R. D. Lowe, M. Jayaraman, D. L. Anderson, *J. Org.Chem.* **1993**, *58*, 904–912.
[30] J. Y. Song, N. Stingelin, W. P. Gillin, T. Kreouzis, *Appl. Phys. Lett.* **2008**, *93*, 233306-1–233306-3.
[31] T. A. Chen, X. M. Wu, R. D. Rieke, *J. Am. Chem. Soc.* **1995**, *117*, 233–244.
[32] A. Kumar, M. A. Baklar, K. Scott, T. Kreouzis, N. Stingelin_Stutzmann, *Adv. Mater.* **2009**, *21*, 4447–4451.
[33] G. Sauve, R. D. McCullough, *Adv. Mater.* **2007**, *19*, 1822–1825.
[34] M. C. Iovu, R. Zhang, J. R. Cooper, D. M. Smilgies, A. E. Javier, E. E. Sheina, T. Kowaleski, R. D. McCullough, *Macromol. Rapid Commun.* **2007**, *28*, 1816–1824.
[35] S. Y. Choi, J. U. Lee, W. Jin, S. Lee, Y. J. Song, W. H. Jo, S. H. Kim, *Macromolecules* **2011**, *44*, 1771–1774.
[36] X. Yu, K. Xiao, J. Chen, N. V. Lavrik, K. Hong, B. G. Sumpter, D. B. Geohegan, *ACS Nano* **2011**, *5*, 3559–3567.
[37] R. D. McCullough, R. D. Lowe, *Chem. Commun.* **1992**, *1*, 70–72.

[38] C. M. Kassis, J. K. Steehler, D. E. Betts, Z. B. Guan, T. J. Romack, J. M. DeSimone, R. W. Linton, *Macromolecules* **1996**, *29*, 3247–3254.
[39] H. Yokoyama, K. Tanaka, A. Takahara, T. Kajiyama, K. Sugiyama, A. Hirao, *Macromolecules*, **2004**, *37*, 939–945.
[40] N. M. L. Hansen, K. Jankova, S. Hvilsted, *Europ. Poly. J.* **2007**, *43*, 255–293.
[41] D. Haynes, A. K. Naskar, A. Singh, C.-C. Yang, K. Burg, G. Harrison, D. W. Smith Jr., *Macromolecules* **2007**, *40*, 9354–9360.
[42] A. Singh, A. K. Naskar, D. Haynes, M. J. Drews, D. W. Smith Jr., *Polym. Bull.* **2011**, *60*, 507–516.
[43] F. Babudri, G. M. Farinola, F. Naso, R. Ragni, *Chem. Comm.* **2007**, 1003–1022.
[44] B. Wang, S. Watt, M. Hong, B. Domercq, R. Sun, B. Kippelen, D. M. Collard, *Macromolecules* **2008**, *41*, 5156–5165.
[45] M. Nicolas, F. Guittard, S. Geribaldi, *Angew. Chem. Int. Ed.* **2006**, *45*, 2251–2254.
[46] M. Jeffries-El, G. Sauve, R. D. McCullough, *Adv. Mater.* **2004**, *16*, 1017–1019.
[47] M. C. Iovu, M. jeffries-El, E. E. Sheina, J. R. Cooper, R. D. McCullough, *Polym. Int.* **2005**, *46*, 8582–8586.
[48] A. B. Koren, M. D. Curtis, A.H. Francis, J. W. Kampf, *J. Am. Chem. Soc.* **2003**, *125*, 5040–5050.
[49] M. D. Curtis, J. Cao, J. W. Kampf, *J. Am. Chem. Soc.* **2004**, *126*, 4318–4328.
[50] J. Cornil, D. Beljonne, J. P. Calbert, J. L. Bredas, *Adv. Mater.* **2001**, *13*, 1053–1067.
[51] J. Cornil, D. Santos, X. Crispin, R. Silbey, J. L. Bredas, *J. Am. Chem. Soc.* **1998**, *120*, 1289–1299.
[52] F. C. Spano, *J. Chem. Phys.* **2005**, *122*, 234701–234715.
[53] F. C. Spano, *J. Chem. Phys.* **2007**, *126*, 159901.
[54] J. Liu, R. Zhang, I. Osaka, S. Mishra, A. Javier, D. Smilgies, T. Kowalewski, R. D. McCullough, *Adv. Funct. Mater.* **2009**, *19*, 3427–3434.
[55] C. B. Tang, A. Tracz, M. Kruk, R. Zhang, D. M. Smilgies, K. Matyjaszewski, T. Kowalewski, *J. Am. Chem. Soc.* **2005**, *127*, 6918–6919.
[56] R. J. Kline, M. D. McGehee, M. F. Toney, *Nat. Mater.* **2006**, *5*, 222–228.
[57] S. Grecu, A. Roggenbuck, A. Opitz, W. Brutting, *Org. Electron.* **2006**, *7*, 276–286.